

UGMRT OBSERVATIONS OF THE GIANT FOSSIL RADIO LOBE IN THE OPHIUCHUS GALAXY CLUSTER

S. Giacintucci¹, M. Markevitch², and T. E. Clarke¹

RESUMEN

El aumento de la temperatura en el núcleo galáctico activo (AGN) central es el mecanismo principal para evitar el enfriamiento radiativo sin control del gas en los centros de los cúmulos de galaxias. Este mecanismo requiere que los jets del AGN transfieran su energía mecánica al gas del intracúmulo de forma suave y autorregulada. El cúmulo Ophiuchus ofrece un ejemplo extraordinario fuera del escenario de retroalimentación suave de AGN. Alberga una enorme cavidad de rayos X fósil de espectro pronunciado descubierta a bajas frecuencias en ondas de radio. Debe haber sido alimentado por el estallido más potente de un AGN conocido hasta ahora en un cúmulo de galaxias, el cual debe haber destruido el núcleo frío del cúmulo. Aquí presentamos nuevas observaciones de este lóbulo fósil en ondas de radio a bajas frecuencias tomadas con el Giant Metrewave Radio Telescope en su versión mejorada. Nuestras imágenes revelan una red de filamentos en radio de origen incierto, con un espectro ($\alpha \sim 2 - 3$) más pronunciado que la emisión circundante ($\alpha \sim 1 - 2$). En el espectro en radio de la región más brillante del lóbulo, encontramos una brecha espectral producida por las pérdidas de energía radiativa. A partir de esta brecha, estimamos que el estallido del AGN se produjo hace aproximadamente 200 Myr.

ABSTRACT

Heating from the central active galactic nucleus (AGN) is the favored mechanism to prevent runaway radiative cooling of the gas in the cores of galaxy clusters. This mechanism requires the AGN jets to transfer their mechanical energy to the intracluster gas in a gentle and self-regulated manner. The Ophiuchus cluster offers a dramatic example outside the gentle AGN feedback scenario. It hosts an enormous X-ray cavity filled by a steep-spectrum fossil radio lobe discovered at low radio frequencies. It should have been inflated by the most powerful AGN outburst known in a galaxy cluster, which should have destroyed the cluster cool core. Here, we present new observations of this fossil radio lobe at low frequencies with the upgraded Giant Metrewave Radio Telescope. Our images reveal a network of radio filaments of uncertain origin, with a radio spectrum ($\alpha \sim 2 - 3$) steeper than the surrounding diffuse emission ($\alpha \sim 1 - 2$). In the radio spectrum of the brightest region of the lobe, we find a spectral break driven by radiative energy losses. From this break, we estimate that the AGN outburst has occurred approximately 200 Myr ago.

Key Words: galaxies: clusters: general — galaxies: clusters: individual (Ophiuchus) — radio continuum: general — radio continuum: galaxies

1. INTRODUCTION

Clusters of galaxies — the most massive gravitationally-bound systems in the Universe — are filled with hot ($T \sim 10^7-8$ K or $kT \sim 1 - 10$ keV) X-ray emitting plasma, called the intracluster medium (ICM), which is their dominant baryonic component, with the mass several times that of the galaxies. Through most of the cluster volume, the radiative cooling time of the ICM is much longer than the age of the cluster. An exception is the cores of clus-

ters with sharply peaked density profiles, marked by giant cD galaxies (e.g., Jones & Forman 1984; Peres et al. 1998), which constitute roughly a third of all clusters. In these systems, the plasma temperature within the inner $r \sim 100$ kpc region ($\sim 5\%$ of the cluster virial radius) drops rapidly inward (e.g., Vikhlinin et al. 2005), while the density sharply increases. This makes for a very X-ray luminous core, with a radiative cooling time shorter than the cluster's age. Such a core is thermally unstable — as the plasma cools, it gets denser to maintain the pressure, and cools ever more rapidly. Eventually it should turn into molecular gas and stars at a rate up to a thousand M_{\odot}/yr . While observational evidence for molecular clouds and filaments condensing out of the

¹Naval Research Laboratory, 4555 Overlook Avenue SW, Code 7213, Washington, DC 20375, USA (simona.giacintucci@nrl.navy.mil, tracy.clarke@nrl.navy.mil).

²NASA/Goddard Space Flight Center, Greenbelt, MD 20771, USA (maxim.markevitch@nasa.gov).

hot phase is growing (e.g., Edge 2001; Salomé et al. 2006; Pulido et al. 2018; Vantyghem et al. 2019), the mass of “warm” gas just below $kT \sim 1$ keV in clusters with some of the highest cooling rates is only a few percent of the amount predicted by the above simple physical picture (e.g., Peterson & Fabian 2006).

Since X-ray cooling is directly observed by the X-ray telescopes, a compensatory steady heating mechanism is required to prevent the formation of such thermal instability. The currently preferred mechanism is the “radio-mode” feedback from the active galactic nucleus (AGN) hosted by the cluster central galaxy (see e.g., Hlavacek-Larrondo et al. 2022, for a review). In this scenario, the mechanical energy released by AGN jet activity, which is fed by the cooling gas, inflates radio bubbles and cavities in the X-ray gas, providing a gentle, steady, and self-regulated heating of the cool gas (e.g., Fabian 2012; McNamara, & Nulsen 2012; Voit et al. 2015; Gaspari et al. 2017). The precise mechanism by which the AGN transfers energy to the ICM throughout the cool core is still poorly understood. It is also unclear whether AGN heating always occurs “gently.” In some systems, in fact, there is evidence for episodes of violent AGN heating, e.g., via large-scale shocks, with notable examples in Hydra A (Nulsen et al. 2005; Wise et al. 2007) and MS 0735.6+7421 (McNamara et al. 2005). Furthermore, violent AGN outbursts, such as Hydra A and MS 0735.6+7421, appear to have deposited most of their enormous mechanical energy ($10^{60} - 10^{61}$ ergs) well beyond the central cooling region, raising the question of how these extraordinary events fit into the AGN feedback scenario to stabilize the cluster cores — it is the central, densest gas that is the most problematic.

The Ophiuchus cluster — the second brightest X-ray cluster in the sky — offers an even more dramatic example outside the gentle AGN feedback scenario. The *Chandra* X-ray image of the cluster revealed a prominent concave surface brightness edge just outside the cool core (Werner et al. 2016, hereafter W16). It appears to be an inner wall of an enormous X-ray cavity $\sim 400 - 500$ kpc in diameter. Using high-sensitivity radio observations at low frequencies from the Giant Metrewave Radio Telescope (GMRT) and images from the Murchison Widefield Array (MWA) GLEAM survey³, Giacintucci et al. (2020; hereafter G20) discovered a giant, steep-spectrum fossil radio lobe that fills this putative X-ray supercavity. The most likely explanation

offered by G20 is the past outburst of the AGN in the center of the Ophiuchus cluster. The energy required to displace the gas and create this cavity would be several 10^{61} erg (W16), making it the most powerful AGN outburst seen in any galaxy cluster (G20).

A set of our recent *XMM-Newton* X-ray observations of that region revealed a candidate weak shock front in the ICM on the outer side of the cavity, presumably driven by the expansion of the radio lobe as it inflated the giant cavity (Giacintucci et al. in preparation). As in other big cavity systems with associated large-scale shocks (e.g., Hydra A, MS 0735.6+7421), this detection indicates a rather violent interaction between the AGN and ICM, raising the question of how the cool core may have survived such a strong episode of AGN heating (G20).

Here, we present a deep radio follow-up of this enormous fossil using the upgraded GMRT (uGMRT). The new observations allow us to map the faintest radio emission in the cavity, study the radio spectral properties of the lobe, and estimate its age using the radio spectrum.

We use a Λ CDM cosmology with $H_0=70$ km s⁻¹ Mpc⁻¹, $\Omega_m = 0.3$ and $\Omega_\Lambda = 0.7$. At the redshift of Ophiuchus ($z = 0.028$), $1'' = 0.562$ kpc. All errors are quoted at the 68% confidence level. The radio spectral index α is defined according to $S_\nu \propto \nu^{-\alpha}$, where S_ν is the flux density at the frequency ν .

2. RADIO OBSERVATIONS

We observed Ophiuchus with the uGMRT in Band 2 (B2, 125–250 MHz) and Band 3 (B3, 300–500 MHz) in May 2018, for a total of 9 hours (7.5 hours on target) in each band. The data were recorded with a bandwidth of 200 MHz, 8192 frequency channels and an integration time of 4 seconds. We reduced the data using the Source Peeling and Atmospheric Modeling (SPAM) pipeline (Intema et al. 2017) adopting a standard calibration scheme of bandpass and gain calibration and direction-independent self-calibration, followed by direction-dependent self-calibration. The flux density scale was set using 3C 48 and Scaife & Heald (2012). Final images were made at the central frequencies of 147, 210 and 400 MHz using joint-channel and multi-scale deconvolution in WSClean (Offringa et al. 2014). Primary beam correction was applied following the GMRT guidelines for B3⁴ and for the images at 147 and 210 MHz⁵. The systematic am-

⁴<http://www.ncra.tifr.res.in/ncra/gmrt/gmrt-users/observing-help/ugmrt-primary-beam-shape>

⁵<http://www.ncra.tifr.res.in:8081/~ngk/primarybeam/beam.html>

³Galactic and Extragalactic All-sky MWA survey (Hurley-Walker et al. 2017).

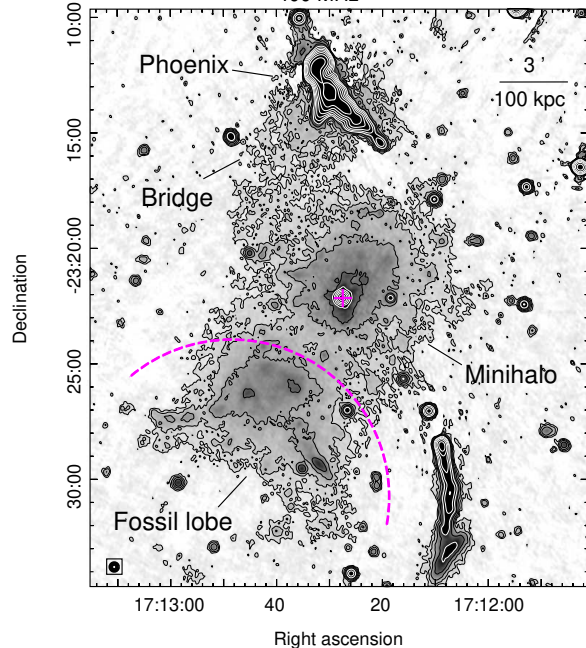


Fig. 1. uGMRT 400 MHz image of the Ophiuchus cluster. The region is $25' \times 25'$ (0.8 Mpc^2) and the cluster center is marked by a cross. The dashed arc traces the X-ray edge (W16, G20). The beam size is $18''$ (bottom-left corner) and the noise is $1\sigma = 25 \mu\text{Jy beam}^{-1}$. Contours are spaced by a factor of 2 starting from $+5\sigma$.

plitude uncertainty was assumed to be 15% at all frequencies.

3. RADIO IMAGES

Our new deep uGMRT image at 400 MHz is presented in Fig. 1. The region is $25' \times 25'$ in size, corresponding to 0.8 Mpc^2 . The cluster core is entirely filled by a faint, diffuse radio *minihalo* (Govoni et al. 2009; Murgia et al. 2010; Giacintucci et al. 2019, G20). Minihalos are found in the cool cores of many massive galaxy clusters (e.g., review by van Weeren et al. 2019). Their radio emission likely arises from the reacceleration of old relativistic particles in the ICM by plasma turbulence generated by the sloshing motions within the cool cores (ZuHone et al. 2013; Brunetti & Jones 2014). North of the core, a bright elongated source is believed to be a radio *phoenix* (W16, G20), i.e., fossil radio plasma (e.g., from past AGN activity) that has been adiabatically compressed and re-energized by the interaction with a shock wave travelling through the ICM (Enßlin & Gopal-Krishna 2001). In these new data, we find that the phoenix and the minihalo seem connected by a faint radio bridge, which suggests a physical link between them — the phoenix may be the source of

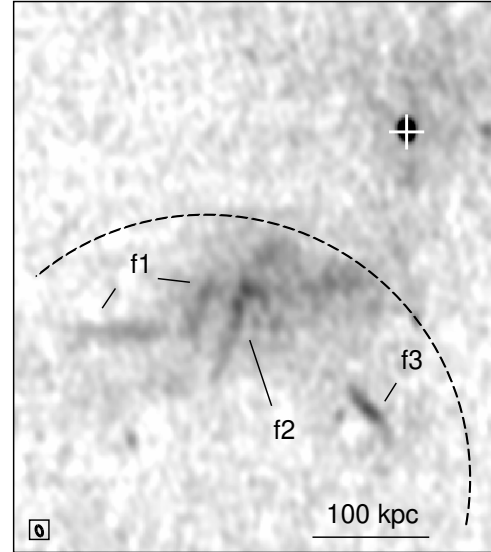


Fig. 2. uGMRT high-resolution images of the fossil lobe at 210 MHz. The cross marks the cluster center and the dashed arc traces the X-ray edge. Filamentary structures within the relic lobe are labelled. The beam is $16'' \times 9''$ (bottom-left corner) and noise is $1\sigma = 0.3 \text{ mJy beam}^{-1}$.

aged electrons that are reaccelerated in the sloshing core.

The magenta arc in Fig. 1 traces the boundary of the cavity detected in the *Chandra* and *XMM-Newton* X-ray images (W16, G20). The fossil radio lobe is seen inside the X-ray edge. Fig. 2 presents a high-resolution 210 MHz image of the innermost and brightest region of the lobe, near the X-ray edge, which exhibits a complex and irregular radio morphology. In particular, a network of narrow ($\sim 5\text{--}10 \text{ kpc}$) and long ($\sim 70\text{--}100 \text{ kpc}$) filaments are embedded in projection within the lobe diffuse emission, with the most prominent labelled f1, f2 and f3. These filaments are also detected in high-resolution images at 147 and 400 MHz (not shown here).

In Fig. 3, we show a lower-resolution image at 400 MHz (black contours) to emphasize the extended emission. Compact sources were identified at the highest resolution ($\sim 6''$; not shown) and subtracted from the *uv* data. The high sensitivity of the image in Fig. 3 allows us to trace the faintest emission from the fossil lobe out to a distance of $\sim 700 \text{ kpc}$ from the X-ray edge ($\sim 820 \text{ kpc}$ from the cluster center). Extended emission to a similar radius is also detected by the MWA GLEAM images at lower frequencies (G20). One of the GLEAM images, for the central frequency of 76 MHz, is also shown in Fig. 3.

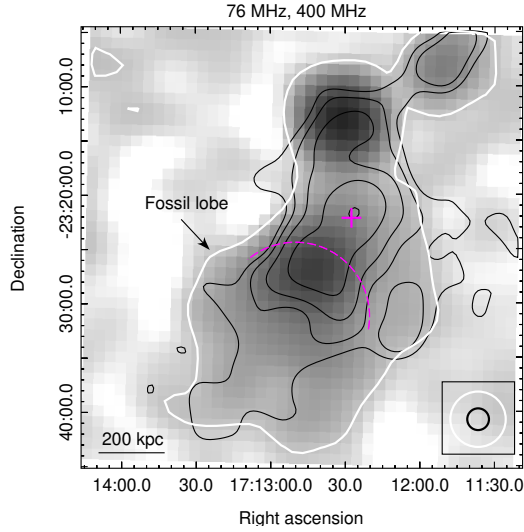


Fig. 3. uGMRT 400 MHz low-resolution contours (black) of the extended emission after subtraction of compact sources from the uv data. The uGMRT contours are overlaid on the GLEAM 76 MHz image (gray scale and the white contour at $200 \text{ mJy beam}^{-1}$). Beams are $2'$ (uGMRT, black circle) and $5'$ (GLEAM, white circle). The uGMRT contours scale by a factor 2 from $3\sigma = 2.3 \text{ mJy beam}^{-1}$.

4. RADIO SPECTRAL ANALYSIS

An integrated radio spectrum of the fossil lobe was presented by G20. It was found it to be well described by a power law with a very steep slope $\alpha_{\text{tot}} = 2.4$. In Fig. 4, we show an updated spectrum that includes our new measurements at 210 MHz and 400 MHz (blue data points) within the same region of the lobe as in G20. The solid line is the best-fit power law with slope $\alpha_{\text{tot}} = 2.37^{+0.15}_{-0.13}$, in agreement with the best-fit slope in G20.

We also computed the integrated spectrum of the innermost region of the lobe using a set of images at 147, 194 and 227 MHz (from the B2 data) and at 333, 416 and 469 MHz (from B3). All images were made with a common uv range ($0.04 - 14 \text{ k}\lambda$) and resolution ($24''$). The flux density of the inner lobe region was measured within the black polygon in Fig. 5(a). The white boxes were used to measure the flux density in the bright filament regions. In Figure 5(b), we show the spectrum of the lobe with filaments included (red) and masked out (black). Both spectra have curved shape with $\alpha_{\text{low}} = 1.1 \pm 0.5$ between 147 MHz and 227 MHz (0.8 ± 0.5 , if the filaments are excised) and $\alpha_{\text{high}} = 2.3 \pm 0.3$ (2.1 ± 0.3) in the range 227–469 MHz. The filaments account for $\sim 30\%$ of the total emission at 147 MHz, their contribution gradually decreasing with increasing frequency,

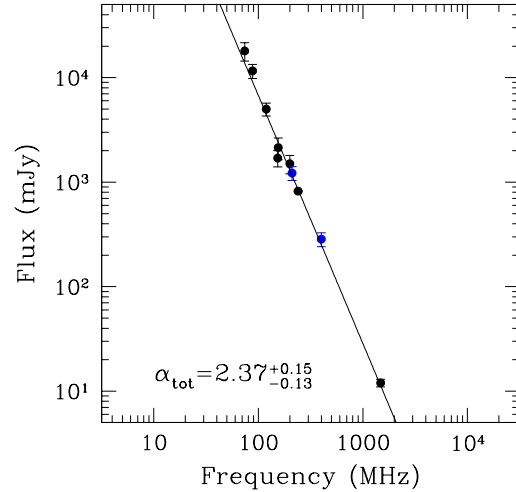


Fig. 4. Integrated radio spectrum of the fossil lobe between 74 MHz and 1477 MHz, adapted from G20. The new uGMRT points at 210 MHz and 400 MHz are in blue. The solid line is the best-fit power law, whose slope is also reported. All flux densities were re-scaled to a common flux scale using the Perley & Butler (2017) scale.

from $\sim 18\%$ at 194 MHz to $\sim 2\%$ at 469 MHz. This is reflected in a flattening of the spectral index of the lobe when the filaments are masked out. Correspondingly, the filaments have a spectral index significantly steeper than that of the diffuse lobe, with $\alpha_{\text{low}} = 1.4 \pm 0.5$ (f1), 1.9 ± 0.7 (f2) and 2.3 ± 0.5 (f3) between 147 and 227 MHz and $\alpha_{\text{high}} = 3.0 \pm 0.3$ (f1), 3.2 ± 0.5 (f2) and 2.7 ± 0.4 (f3) between 227 and 469 MHz.

We modeled both spectra of the lobe inner region in Fig. 5(b) using a Jaffe-Parola synchrotron model (JP; Jaffe & Perola 1973), which assumes a single injection of relativistic electrons with an initial power-law distribution. After the initial injection event, as the radiating electrons undergo energy losses, a cut-off develops in their energy spectrum, which leads to an exponential cut-off in the emitted spectrum beyond a break frequency ν_{br} . It is assumed that the radiative energy losses are dominant with respect to other processes (e.g., adiabatic losses), that electron density and magnetic field are homogeneous within the emitting volume and that the electron pitch angle is isotropic only on short timescales relative to the radiative lifetime (i.e., the synchrotron losses are statistically the same for all electrons). The JP best fits are shown as solid lines in Fig. 5(b). We adopted an injection spectral index of $\alpha_{\text{inj}} = 0.5$. The model fits well both spectra ($\chi_{\text{red}}^2 = 0.5$) and provides a break frequency $\nu_{\text{br}} = 286^{+63}_{-51} \text{ MHz}$ (with filaments)

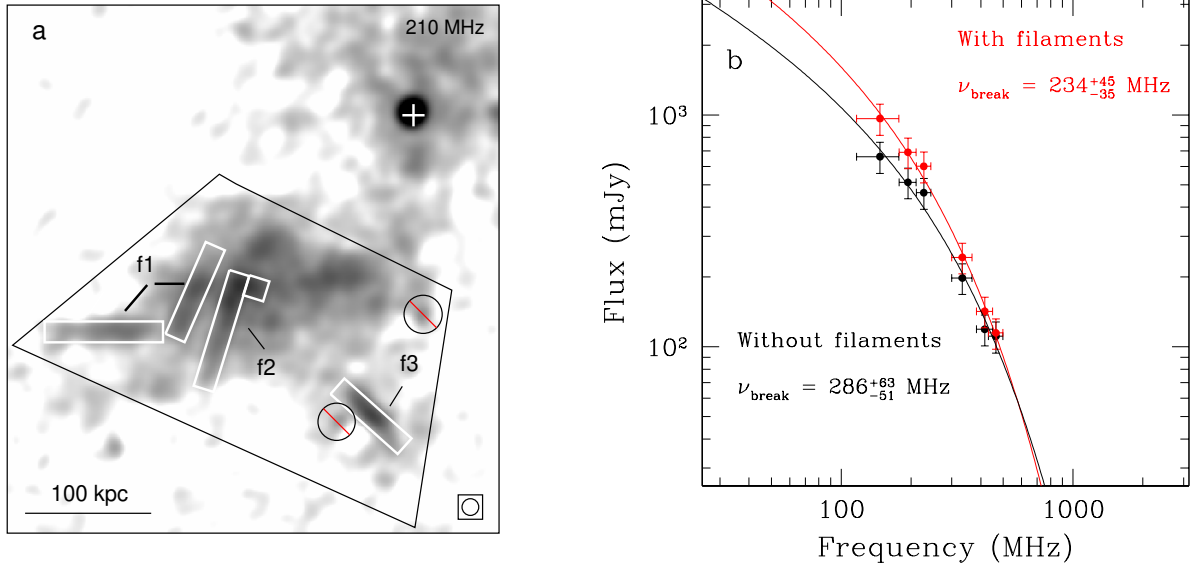


Fig. 5. (a) 210 MHz image of the lobe inner region at $24''$ resolution (bottom-right corner). The filaments are labelled. The black polygon marks the region used to compute the spectra shown in (b). The white regions are used to measure the flux density of the filaments. Two compact sources are masked out. The white cross marks the cluster center. (b) Integrated radio spectrum of the lobe inner region between 147 MHz and 469 MHz, computed using the black region shown in (a) and with filaments included (red) and subtracted (black). The solid curves are the best-fit JP models (see text). The best-fit break frequencies are also reported.

and 234^{+45}_{-35} MHz (without filaments).

5. AGE OF THE FOSSIL LOBE

An estimate of the synchrotron (or “spectral”) age of a radio source can be estimated from the break frequency ν_{br} in the radio spectrum, which arises because of the radiative energy loss (e.g., Eq. 4 in the review paper by Hardcastle & Croston 2020).

As discussed in G20 and above, the integrated radio spectrum of the Ophiuchus fossil lobe is a single power law between 74 and 1477 MHz, with no evidence for a spectral break. However, exploiting the wide band and high sensitivity of our new uGMRT observations, we were able to measure and model the spectrum of its innermost region (within ~ 200 kpc from the X-ray edge) between 147 and 469 MHz (Fig. 5) and find a spectral break at $\sim 230 - 290$ MHz. From this value, and assuming a magnetic field strength of $B \sim 5 \mu\text{G}$ ⁶, we derive an age $t_{rad} \sim 180 - 200$ Myr. Since we assumed that the observed steepening in the spectrum is merely due to electron aging in a magnetic field that is constant and uniform across the lobe and neglected the effects of any expansion/compression of the radio plasma, re-acceleration and mixing with the ICM, the age calculated above is very approximate (e.g., Blundell

& Rawlings 2001). A detailed calculation that includes these effects is beyond the scope of the present work. However, this estimate supports the interpretation that the radio plasma in the giant X-ray cavity is very old.

The age of the Ophiuchus lobe is at the high end of the range of spectral ages typically inferred for dying/remnant radio galaxies (e.g., Parma et al. 2007; Jamroz et al. 2004; Giacintucci et al. 2007; Murgia et al. 2011; Shulevski et al. 2017; Brienza et al. 2018; Maccagni et al. 2020). Recently, similarly long radiative ages ($\sim 250 - 350$ Myr) have been reported for AGN remnant plasma that was discovered at low radio frequencies in the galaxy groups NGC 507 (Brienza et al. 2022) and Nest200047 (Brienza et al. 2021) and in the cluster A 2877 (Hodgson et al. 2021). Such long ages raise the question of how the radio emission can still be detectable by radio telescopes. The radiative losses, combined with adiabatic expansion, would lead the fossil plasma to fade out of the radio band on a relatively short timescale (few 10^7 years; e.g., English et al. 2019). A possible reason is that the radio plasma in these objects and in Ophiuchus is confined by the surrounding ICM, which limits its adiabatic expansion.

⁶The inverse Compton equivalent magnetic field is $B_{IC} = 3.25(1+z)^2 = 3.43 \mu\text{G}$ at the redshift of Ophiuchus.

6. ORIGIN OF THE FILAMENTS

Filamentary features are often seen within the extended lobes of radio galaxies (e.g., Perley et al. 1984; Owen et al. 2000; Laing et al. 2011; Wykes et al. 2014; Hardcastle et al. 2019; Gendron-Marsolais et al. 2021; Maccagni et al. 2020; Brienza et al. 2021). These structures may be tracing magnetic field variations within the lobes and/or irregularities in the distribution of the relativistic electrons (e.g., Hardcastle 2013). Magneto-hydrodynamical (MHD) turbulence and plasma instabilities within the lobes may also lead to a filamentary structure in synchrotron emission (e.g. Eilek 1989; Hardcastle 2013; Wykes et al. 2013, Jun & Norman 1995; Ryu, Jones & Frank 2000).

In the Ophiuchus lobe, the radio filaments appear as narrow (5-10 kpc) and long (70-100 kpc) strands embedded inside the inner region of the fossil lobe. Their spectral index is extremely steep ($\alpha \sim 2 - 3$), steeper than the underlying smoother lobe emission ($\alpha \sim 1 - 2$). This is different from what is generally seen in other radio galaxies, where the filaments usually have a flatter spectrum compared to that of the surrounding plasma (e.g., Hercules A, Timmerman et al. 2022). A striking example is the remnant radio galaxy in Nest200047 (Brienza et al. 2021), whose fossil lobes (with α as steep as 2.5) contain a network of flatter-spectrum filaments (down to $\alpha \sim 0.8$). A flatter spectral index may indicate compression of the radio-emitting plasma inside the filaments, e.g., by ICM motions or weak shocks. Compression would, in fact, increase the synchrotron luminosity and cause a shift of the spectral cut-off to higher frequencies with respect to simple radiative aging predictions. A flatter spectral index would also be expected if the filaments were merely mapping the regions of enhanced magnetic field (Tribble 1994). The steeper index of the filaments in the Ophiuchus lobe is not consistent with these interpretations.

A notable case that may be somewhat similar to Ophiuchus is the Centaurus A, where a complex structures of bright 30 – 50 kpc long filaments is embedded within the giant lobes of the radio galaxy (e.g. Feain et al. 2011). The spectral index of the filaments ($\alpha \sim 0.8$) is slightly steeper than the spectrum of the lobe emission ($\alpha \sim 0.5 - 0.7$; Wykes et al. 2014). The steeper index of the filaments appears to rule out scenarios in which the higher synchrotron emissivity in the filaments is driven by large-scale efficient particle acceleration (e.g., via strong shocks). It was instead argued that the filaments may be generated by MHD turbulence within the lobe volume, possibly driven by current (or recently stopped) jet

activity (Wykes et al. 2014). Numerical simulations show that MHD turbulence can lead to the formation of filaments in which the magnetic field is stretched and amplified (e.g., Tregillis, Jones & Ryu 2005, Schekochihin et al. 2004, Hardcastle 2013). Given the very steep spectral index and large spectral age of the fossil lobe in Ophiuchus, the jet activity has presumably stopped a long time ago. In this case, the development of turbulence within the buoyant fossil lobe may be related to the hydrodynamics of the bubble rising and/or expanding into the ICM. However, such turbulence would also lead to the disruption of the bubble, which we do not observe.

7. CONCLUSIONS

New high-sensitivity, high-resolution observations of the Ophiuchus fossil radio lobe at low frequencies with uGMRT reveal intricate spatial structure. We find narrow radio filaments of uncertain origin with a spectrum steeper than the surrounding diffuse emission. The spectrum of the brightest region of the radio lobe exhibits a break, from which we estimate an age of the radio source of ~ 200 Myr — this is when this most powerful known AGN explosion has occurred.

The Ophiuchus fossil may be an early example of a new radio phenomenon, waiting to be uncovered in other galaxy clusters by the ongoing high-sensitivity surveys at frequencies of ~ 1 GHz and below (e.g., with LOFAR, MWA, MeerKAT, ASKAP) and by future sensitive radio telescopes, such as the Square Kilometre Array. Their associated cavities in the cluster X-ray gas are large and have very low X-ray surface brightness contrast, since they will be located outside the bright central core. Their detection would require observations with X-ray telescopes with high angular resolution and large collecting area for the needed photon statistics. The future Athena’s Wide-Field Imager and NASA’s prospective AXIS Probe and STAR-X Explorer should be able to detect such low-contrast X-ray cavities outside the cluster cores.

Acknowledgements: Basic research in radio astronomy at the Naval Research Laboratory is supported by 6.1 Base funding. We thank the staff of the GMRT who made these observations possible. GMRT is run by the National Centre for Astrophysics of the Tata Institute of Fundamental Research.

REFERENCES

Blundell, K. M. & Rawlings, S. 2001, *Particles and Fields in Radio Galaxies Conference*, 250, 363

- Brienza, M., Morganti, R., Murgia, M., et al. 2018, *A&A*, 618, A45
- Brienza, M., Shimwell, T. W., de Gasperin, F., et al. 2021, *Nature Astronomy*, 5, 1261
- Brienza, M., Lovisari, L., Rajpurohit, K., et al. 2022, *A&A*, 661, A92
- Brunetti, G., & Jones, T. W. 2014, *International Journal of Modern Physics D*, 23, 1430007
- Edge, A. C. 2001, *MNRAS*, 328, 762
- Eilek, J. A. 1989, *AJ*, 98, 256
- English, W., Hardcastle, M. J., & Krause, M. G. H. 2019, *MNRAS*, 490, 5807
- Enßlin, T. A. & Gopal-Krishna 2001, *A&A*, 366, 26
- Fabian, A. C. 2012, *ARA&A*, 50, 455
- Feain, I. J., Cornwell, T. J., Ekers, R. D., et al. 2011, *ApJ*, 740, 17
- Gaspari, M., Temi, P., & Brighenti, F. 2017, *MNRAS*, 466, 677
- Gendron-Marsolais, M.-L., Hull, C. L. H., Perley, R., et al. 2021, *ApJ*, 911, 56
- Giacintucci, S., Venturi, T., Murgia, M., et al. 2007, *A&A*, 476, 99
- Giacintucci, S., Markevitch, M., Cassano, R., et al. 2019, *ApJ*, 880, 70
- Giacintucci, S., Markevitch, M., Johnston-Hollitt, M., et al. 2020, *ApJ*, 891, 1 (G20)
- Govoni, F., Murgia, M., Markevitch, M., et al. 2009, *A&A*, 499, 371 (G09)
- Hardcastle, M. J. 2013, *MNRAS*, 433, 3364
- Hardcastle, M. J., Croston, J. H., Shimwell, T. W., et al. 2019, *MNRAS*, 488, 3416
- Hardcastle, M. J. & Croston, J. H. 2020, *New Astronomy Rev.*, 88, 101539
- Hlavacek-Larrondo, J., Li, Y., & Churazov, E. 2022, *Handbook of X-ray and Gamma-ray Astrophysics*. Edited by Cosimo Bambi and Andrea Santangelo, 5
- Hodgson, T., Bartalucci, I., Johnston-Hollitt, M., et al. 2021, *ApJ*, 909, 198
- Hurley-Walker, N., Callingham, J. R., Hancock, P. J., et al. 2017, *MNRAS*, 464, 1146
- Intema, H. T., Jagannathan, P., Mooley, K. P., et al. 2017, *A&A*, 598, A78
- Jaffe, W. J. & Perola, G. C. 1973, *A&A*, 26, 423
- Jamrozy, M., Klein, U., Mack, K.-H., et al. 2004, *A&A*, 427, 79
- Jones, C. & Forman, W. 1984, *ApJ*, 276, 38
- Jun, B.-I., Norman, M. L., & Stone, J. M. 1995, *ApJ*, 453, 332
- Laing, R. A., Guidetti, D., Bridle, A. H., et al. 2011, *MNRAS*, 417, 2789
- Maccagni, F. M., Murgia, M., Serra, P., et al. 2020, *A&A*, 634, A9
- McNamara, B. R., Nulsen, P. E. J., Wise, M. W., et al. 2005, *Nature*, 433, 45
- McNamara, B. R., & Nulsen, P. E. J. 2012, *New Journal of Physics*, 14, 055023
- Murgia, M., Eckert, D., Govoni, F., et al. 2010, *A&A*, 514, A76
- Murgia, M., Parma, P., Mack, K.-H., et al. 2011, *A&A*, 526, A148
- Nulsen, P. E. J., McNamara, B. R., Wise, M. W., & David, L. P. 2005, *ApJ*, 628, 629
- Offringa, A. R., McKinley, B., Hurley-Walker, N., et al. 2014, *MNRAS*, 444, 606
- Owen, F. N., Eilek, J. A., & Kassim, N. E. 2000, *ApJ*, 543, 611
- Parma, P., Murgia, M., de Ruiter, H. R., et al. 2007, *A&A*, 470, 875
- Peres, C. B., Fabian, A. C., Edge, A. C., et al. 1998, *MNRAS*, 298, 416
- Perley, R. A., Dreher, J. W., & Cowan, J. J. 1984, *ApJ*, 285, L35
- Perley, R. A., & Butler, B. J. 2017, *ApJS*, 230, 7
- Peterson, J. R. & Fabian, A. C. 2006, *Phys. Rep.*, 427, 1
- Pulido, F. A., McNamara, B. R., Edge, A. C., et al. 2018, *ApJ*, 853, 177
- Salomé, P., Combes, F., Edge, A. C., et al. 2006, *A&A*, 454, 437
- Scaife, A. M. M., & Heald, G. H. 2012, *MNRAS*, 423, L30
- Schekochihin, A. A., Cowley, S. C., Taylor, S. F., et al. 2004, *ApJ*, 612, 276
- Shulevski, A., Morganti, R., Harwood, J. J., et al. 2017, *A&A*, 600, A65
- Timmerman, R., van Weeren, R. J., Callingham, J. R., et al. 2022, *A&A*, 658, A5
- Tregillis, I. L., Jones, T. W., & Ryu, D. 2004, *ApJ*, 601, 778
- Tribble, P. C. 1994, *MNRAS*, 269, 110
- Vantyghem, A. N., McNamara, B. R., Russell, H. R., et al. 2019, *ApJ*, 870, 57
- van Weeren, R. J., de Gasperin, F., Akamatsu, H., et al. 2019, *Space Sci. Rev.*, 215, 16
- Vikhlinin, A., Markevitch, M., Murray, S. S., et al. 2005, *ApJ*, 628, 655
- Voit, G. M., Donahue, M., Bryan, G. L., et al. 2015, *Nature*, 519, 203
- Werner, N., Zhuravleva, I., Canning, R. E. A., et al. 2016, *MNRAS*, 460, 2752 (W16)
- Wise, M. W., McNamara, B. R., Nulsen, P. E. J., et al. 2007, *ApJ*, 659, 1153
- Wykes, S., Croston, J. H., Hardcastle, M. J., et al. 2013, *A&A*, 558, A19
- Wykes, S., Intema, H. T., Hardcastle, M. J., et al. 2014, *MNRAS*, 442, 2867
- ZuHone, J. A., Markevitch, M., Brunetti, G., & Giacintucci, S. 2013, *ApJ*, 762, 78